Sensors & Transducers, Vol. 263, Issue 4, December 2023, pp. 89-97

Sensors & Transducers
Published by IFSA Publishing, S. L., 2023
http://www.sensorsportal.com

On the Possible Method of Improving Properties of Semiconductor Lasers

[1,*] Marta GLADYSIEWICZ, [2] Marek S. WARTAK
[1] Department of Experimental Physics, Wroclaw University of Science and Technology, 50-370 Wroclaw, Poland
[2] Department of Physics and Computer Science, Wilfrid Laurier University, Waterloo, Ontario N2L3C5, Canada
[1] Tel.: 667 802 532, fax: +48 71 328 36 96
E-mail: marta.gladysiewicz-kudrawiec@pwr.edu.pl

Received: 18 October 2023 / Accepted: 13 December 2023 / Published: 20 December 2023

Abstract: This paper is aimed as a concise, short introduction to semiconductor lasers and a presentation of a specific method to improve optical gain. We start with the short description of lasers and semiconductor lasers, in particular. They play an important role in current technological developments. They found applications in many popular devices and communication systems, like laser printers, DVD players, optical fiber communications, to just name a few. In this paper, we outline fundamentals of semiconductor lasers and concentrate on those based on quantum wells. Properties and operating parameters of those devices can be optimized for a certain application. Here we concentrate on the influence of growth directions on optical gain. We summarized mathematical formalism used to determine band structure and gain and have conducted numerical simulations for various orientations of the crystal.

We illustrate the applicability of our formalism by presenting results (band structure and material gain) for only few high symmetry orientations of the substrate and concentrate on quantum wells fabricated from InGaAsN/GaAs. Modifications of band structure due to rotations significantly affect material gain.

Our approach can also be extended to other semiconductor materials. They can help to design lasers with improved characteristics.

Keywords: Semiconductor lasers, Band structure, Crystallographic orientation, Material gain.

1. Introduction

Generic laser consists of a resonator (cavity) typically formed by two mirrors and gain medium located between mirrors where the amplification of electromagnetic radiation (light) takes place. Such a system is an oscillator analogous to one in electronics. To form an oscillator, an amplifier (where gain is created) and feedback are needed. Feedback is provided by two mirrors which also confine light. One of the mirrors is partially transmitting which allows light to escape from the device. In short, a laser is an oscillator analogous to an oscillator in electronics.

There must be an external energy provided into gain medium (process known as pumping). Most popular (practical) pumping mechanisms are by optical or electrical means.

In this paper we concentrate on important class of lasers, namely semiconductor lasers (SL), see [1, 2] for recent general introduction to SL. They play an important role in today's technological developments. They can be found in popular devices, like iPhones, DVD players and laser printers. In short, semiconductor laser (name laser diode is also often used) is based on p-n junction which is combined with an optical resonator. The p-n junction forms a diode which operates in a forward direction.

2. Basic Facts of Semiconductor Lasers Based on Quantum Wells

Generally, semiconductor lasers (also known as laser diodes) can be broadly classified into two basic types: edge-emitting lasers, or surface-emitting lasers.

A typical edge-emitting laser has the longitudinal direction of the optical cavity oriented perpendicular to the flow direction of electrical current in the device.

On the other hand, in surface-emitting lasers the optical cavity is oriented along flow of electrical current and it is perpendicular to the growth direction. A popular example of the surface emitting laser is the vertical-cavity surface-emitting laser (VCSEL). In this structure the optical cavity is short, on the order of a wavelength of the light. To achieve reasonably low threshold current in such devices the mirrors must have very high reflectivity.

Three-dimensional (3D) view of a generic edge-emitting semiconductor laser (the so-called Fabry-Perot) is shown in Fig. 1.

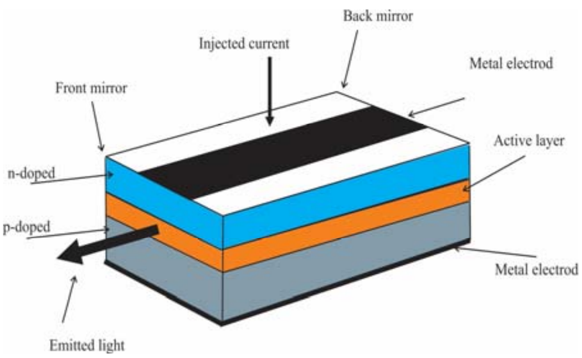

Fig. 1. Schematic of Fabry-Perot laser.

The main element of this structure is associated with the existence of the so-called Fabry-Perot resonator cavity where the optical feedback is provided by the difference in refractive indices between semiconductor structure and external environment.

It is possible to have different types of mirrors as they also provide mode selectivity. Two basic types of SL are distributed feedback (DFB) laser and distributed Bragg reflector (DBR) [3].

In DFB lasers, grating (corrugation) is produced in one of the cladding layers thus creating Bragg reflections at such periodic structure. The structure causes a wavelength sensitive feedback. It should be emphasized that the grating extends over entire laser structure. When one restricts corrugation to the mirror regions only and leaves flat active region in the middle, then the so-called DBR structure is created, which also provides wavelength sensitive feedback.

Every laser structure consists of many layers of various materials, each playing a different role. Those layers are responsible for the efficient transport of electrons and holes from electrodes into an active region and also for confinement of carriers and photons into active region so they can strongly interact.

In semiconductor laser diodes the emission of light is due to the radiative recombination of the electron-hole pairs. Electron-hole pairs are formed by electrons from conduction band (CB) and holes from valence band (VB). Between these bands there exists the forbidden band characterized by bandgap energy.

Typical characteristic of SL is shown in Fig. 2. It shows output power vs driving electric current. The output power degrades fast with increased temperature of the sample.

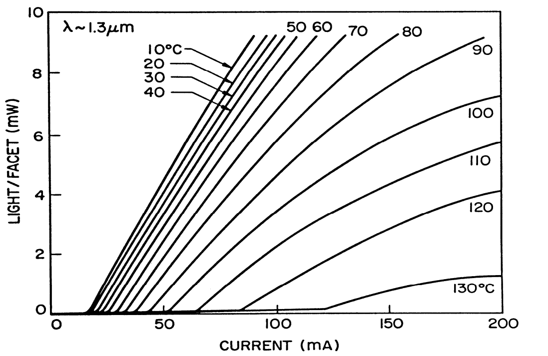

Fig. 2. Typical characteristic of SL showing output power versus current.

Modern SL structures are based on so-called quantum well which form active region and where conduction-valance band transitions are taking place, see Fig. 3.

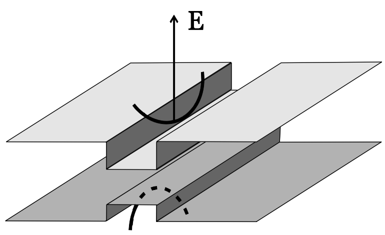

Fig. 3. Schematic of the quantum-well structure.

The structure is formed by two semiconductors with different bandgaps. They create the so-called heterostructure. Carriers (electrons and holes) can move freely within well (their dispersion relation is parabolic) but along direction perpendicular to the well their energies are quantized, see Fig. 4.

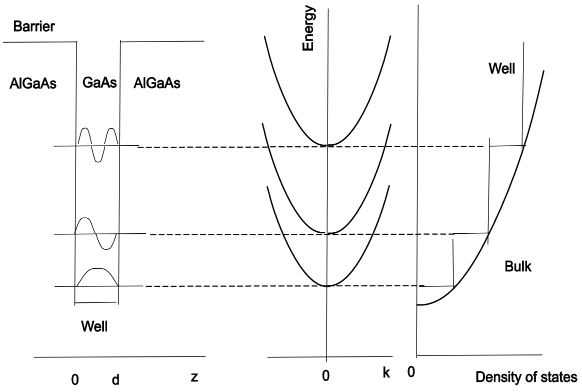

Fig. 4. Schematic of quantization of energies within the quantum-well structure.

3. Methods of Improving Properties (Characteristics) of Semiconductor Lasers

There is a long list of parameters of SL which could be optimized and improved. Over the years there were many efforts towards the improvement of their operating characteristics and also application of new materials. Various compounds and their functionalities have been analyzed in recent years. For example, applications in ultraviolet emitters were recently reviewed by Kudrawiec and Hommel [4].

In this work we briefly concentrate on high-power devices, fast devices (those which are directly modulated) and also on improving (making larger) material (optical) gain.

Fundamental and technological reasons limiting the optical power of SL were analyzed by several groups, see e.g., Tarasov [5]. The design of high-power SL discussed by Tarasov is based on separate-confinement double heterostructures (SC DHs). Often the SC DH is used to confine an electromagnetic wave by a waveguide layer which results in decrease of threshold current density due to decrease of the active region thickness. The use of a quantum-well epitaxial layer as an active region of the laser SC DH allowed one to reduce the threshold current density to 40 A/cm^2 [5].

Another important problem is to increase speed of directly modulated SL [6]. SL can be modulated using two methods: direct modulation or using external modulators (costly approach). Common approach is to directly modulate diode current which leads to appropriately modulated output power.

However, in this approach relaxation oscillations are created. They are characterized by a relaxation-oscillation frequency which describes rate at which energy is exchanged between photon system and carriers. Another limit is introduced by parasitics. As a result, the maximum modulation frequencies range from 1 to 70 GHz, depending on the type of laser and its packaging.

Carrier transport effects are another limiting factor for direct modulation of semiconductor lasers [7]. Optimizing transport of carriers, especially in the multiple quanta well systems results in faster devices. Based on rate equation model it was demonstrated that the tunneling injection mechanism increases the modulation bandwidth of the laser output compared to the classical injection mechanism [7].

Yet, another issue is to increase optical gain of SL. One possible method is to growth samples on rotated substrates. In the following we concentrate on this issue.

It has been known for a long time that the growth of quantum wells (QWs) at the rotated substrates (as opposed to the natural (001) direction) results in the improved properties of semiconductor lasers based on various material systems. Over the years several material systems has been analyzed, both theoretically and experimentally. For a recent summaries of various growth methods, see [8]. Typical discussed material systems were GaAs-AlGaAs and InGaAsP-GaInAs. Theoretical approaches were based on 4- band, 6-band and 8-band Hamiltonians.

On the theoretical side it was concluded that selecting proper orientation of the substrate results in lower (compared to (001) direction) threshold current [9, 10]. It was also determined that differential gain is about 1.6 times larger for the (110)-oriented 1.55 μm strained QWs than for equivalent (001)-oriented QW's [11]. It was also found that linewidth enhancement factor in strained QW laser based on $In_{0.7}Ga_{0.3}As$-InP is smaller for (111) growth direction than in conventional strained QW lasers on (001) substrates [12]. Typical value calculated for the (111) rotated substrate was less than 1.4, much lower than for conventional strained QW lasers on (001) substrates.
In addition to the above material systems, in recent years dilute nitride semiconductors such as InGaAsN attracted wide attention. Their study is motivated by potential applications in GaAs-based laser diodes operating at 1.3 and 1.55 μm. Those material systems are modeled using 10-band Hamiltonians which are combinations of 8-band model and BAC model [13], [14]. Currently, optical and electrical properties including band structure of InGaAsN/GaAs quantum wells (QWs) are well described in the literature. Most of the reported results were focused on the (001)-oriented substrates. Some of the papers for (001) oriented QWs were published by Ng et al [15] and Gladysiewicz et al. [16].

4. Theoretical Approach

4.1. General

To describe the system (laser) we used the kp method. It is based on the following Hamiltonian

$$H = \frac{1}{2m_0}\hat{\boldsymbol{p}}^2 + V(\boldsymbol{r}) + \frac{\hbar}{4m_0^2c^2}\hat{\sigma}\cdot\nabla V\times\hat{\boldsymbol{p}} = \\ = H_0 + H_{SO}, \tag{1}$$

where H_0 is the zeroth-order term and H_{SO} describes spin-orbit interaction. The basic functions are summarized below

$$\begin{aligned}
u_{10}(\vec{r}) &= \left|\frac{3}{2},\frac{3}{2}\right\rangle = \frac{-1}{\sqrt{2}}\left|(X+iY)\uparrow\right\rangle \\
u_{20}(\vec{r}) &= \left|\frac{3}{2},\frac{1}{2}\right\rangle = \frac{-1}{\sqrt{6}}\left|(X+iY)\downarrow\right\rangle + \sqrt{\frac{2}{3}}\left|Z\uparrow\right\rangle \\
u_{30}(\vec{r}) &= \left|\frac{3}{2},\frac{-1}{2}\right\rangle = \frac{1}{\sqrt{6}}\left|(X-iY)\uparrow\right\rangle + \sqrt{\frac{2}{3}}\left|Z\downarrow\right\rangle \\
u_{40}(\vec{r}) &= \left|\frac{3}{2},\frac{-3}{2}\right\rangle = \frac{1}{\sqrt{2}}\left|(X-iY)\downarrow\right\rangle \\
u_{50}(\vec{r}) &= \left|\frac{1}{2},\frac{1}{2}\right\rangle = \frac{1}{\sqrt{3}}\left|(X+iY)\downarrow\right\rangle + \frac{1}{\sqrt{3}}\left|Z\uparrow\right\rangle \\
u_{60}(\vec{r}) &= \left|\frac{1}{2},\frac{-1}{2}\right\rangle = \frac{1}{\sqrt{3}}\left|(X-iY)\uparrow\right\rangle - \frac{1}{\sqrt{3}}\left|Z\downarrow\right\rangle
\end{aligned} \tag{2}$$

4.2. Description of Rotations

Normally, the system is described assuming the z-axis to be perpendicular to the quantum well. In order to describe rotations of the substrate we follow method as described in [17], see Fig. 5. Below, we briefly summarize the approach.

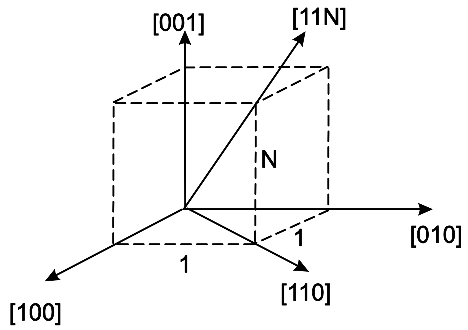

Fig. 5. Relationship of the general [11N] coordinate system to the conventional [001] crystal coordinate system.

We use the following notation for coordinate systems, see Fig. 6: the (x,y,z) is associated with the (001) oriented QW and (1,2,3) coordinate system with arbitrary rotated QW. The growth direction for (001) -oriented substrate is along z axis and along 3 axes for rotated substrate. To obtain rotated Hamiltonian from (001)-oriented Hamiltonian the following rotation matrix is used.

$$U = \begin{bmatrix} \cos\theta\cos\phi & \cos\theta\sin\phi & -\sin\theta \\ -\sin\phi & \cos\phi & 0 \\ \sin\theta\cos\phi & \sin\theta\sin\phi & \cos\theta \end{bmatrix} \tag{3}$$

The matrix has the following properties: $U^T = U^{-1}$, $U^T U = I$ and $U_{ik}U_{jk} = \delta_{ij}$. The components of vectors and tensors transform as

$$\begin{aligned} k'_i &= U_{i\alpha}k_\alpha,\ \varepsilon'_{ij} = U_{i\alpha}U_{j\beta}\varepsilon_{\alpha\beta}, \\ C'_{ijkl} &= U_{i\alpha}U_{j\beta}U_{k\gamma}U_{l\delta}C_{\alpha\beta\gamma\delta}, \end{aligned} \tag{4}$$

where superscripts "-1" means matrix inverse and "T" means matrix transposition. Here ϕ is the angle between x-z and 1-3 planes and θ is the angle between axis z and axis 3. Here k and k' are wave vectors and ε_{ij} and $\varepsilon'_{\alpha\beta}$ are strain tensors for (001) and arbitrary orientation, respectively. In other words, the angles θ and ϕ are Euler rotation angles about axes 2 and z respectively. The angles with respect to (001) direction for (hkl) Miller planes can be obtained by the following relations

$$\theta = \tan^{-1}\frac{\sqrt{h^2+k^2}}{l} \qquad \phi = \tan^{-1}\frac{k}{h} \tag{5}$$

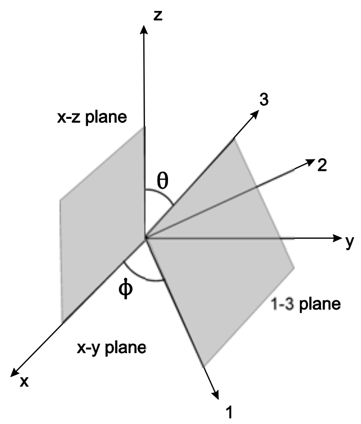

Fig. 6. General transformation for arbitrary rotation from old to new rectangular coordinate system using spherical coordinate system: Axes x, y, z transform to axes 1, 2, 3 respectively, which are perpendicular to each other; x-z and 1-3 planes are indicated.

Transformation matrix leads to the following relation

$$\begin{bmatrix} X' \\ Y' \\ Z' \end{bmatrix} = \begin{bmatrix} & & \\ & U & \\ & & \end{bmatrix} \begin{bmatrix} X \\ Y \\ Z \end{bmatrix} \tag{6}$$

The spins in the original coordinate system are assumed to be along the growth direction z. For rotated system, spins will be rotated by the rotation matrix for spins

$$M_s = \begin{bmatrix} e^{-i\frac{\phi}{2}}\cos\frac{\theta}{2} & e^{i\frac{\phi}{2}}\sin\frac{\theta}{2} \\ -e^{-i\frac{\phi}{2}}\sin\frac{\theta}{2} & e^{i\frac{\phi}{2}}\cos\frac{\theta}{2} \end{bmatrix}, \tag{7}$$

which leads to the following relation

$$\begin{bmatrix} \uparrow' \\ \downarrow' \end{bmatrix} = \begin{bmatrix} e^{-i\frac{\phi}{2}} \cos\frac{\theta}{2} & e^{i\frac{\phi}{2}} \sin\frac{\theta}{2} \\ -e^{-i\frac{\phi}{2}} \sin\frac{\theta}{2} & e^{i\frac{\phi}{2}} \cos\frac{\theta}{2} \end{bmatrix} \begin{bmatrix} \uparrow \\ \downarrow \end{bmatrix} \tag{8}$$

By combining matrices U and M_s we can relate basis functions in rotated coordinate system $\left[X', Y', Z'\right]^T$ with spins $\left[\uparrow', \downarrow'\right]^T$ and basic functions in original coordinate system $\left[X, Y, Z\right]^T$ with spins $\left[\uparrow, \downarrow\right]^T$. Combining matrices U and M_s, we can obtain matrix that relates $\left[X'\uparrow', Y'\uparrow', Z'\uparrow', X'\downarrow', Y'\downarrow', Z'\downarrow'\right]^T$ and $\left[X\uparrow, Y\uparrow, Z\uparrow, X\downarrow, Y\downarrow, Z\downarrow\right]^T$, where superscript T means transposition. The combined matrix is obtained as a Kronecker product $\otimes$ (outer product for matrices) of matrices M_s and U.

$$M_c = M_s \otimes U \tag{9}$$

The matrix M_c leads to the following relation between basis functions

$$\begin{bmatrix} X'\uparrow' \\ Y'\uparrow' \\ Z'\uparrow' \\ X'\downarrow' \\ Y'\downarrow' \\ Z'\downarrow' \end{bmatrix} = \begin{bmatrix} & & \\ & M_c & \\ & & \end{bmatrix} \begin{bmatrix} X\uparrow \\ Y\uparrow \\ Z\uparrow \\ X\downarrow \\ Y\downarrow \\ Z\downarrow \end{bmatrix}, \tag{10}$$

where empty space in square brackets corresponds to matrix M_c. Full form of matrix M_c was provided in [17].

4.3. The Effect of Strain

The strain effects are modeled using Bir and Pikus approach [19]. The strain tensor takes different explicit forms for various strain situations. The strain tensor components are represented by

$$\varepsilon_{xx} = \varepsilon_{yy} = \frac{a_{GaAsBi} - a_{GaAs}}{a_{GaAs}} \tag{11}$$

The form of ε_{zz} varies with orientation, due to the fact that the elastic stiffness tensor is transformed. The relevant expressions are

$$\varepsilon_{zz}^{(001)} = -2\frac{C_{12}}{C_{11}}\varepsilon_{xx}, \tag{12}$$

$$\begin{aligned} \varepsilon_{zz}^{(110)} &= -\frac{3C_{12} + C_{11} - 2C_{44}}{C_{11} + 2C_{12} + 4C_{44}}\varepsilon_{xx}, \\ \varepsilon_{zz}^{(111)} &= -2\frac{C_{11} + 2C_{12} - 2C_{44}}{C_{11} + 2C_{12} + 4C_{44}}\varepsilon_{xx} \end{aligned} \tag{13}$$

Other terms of the strain tensor are equal to zero. The components of Bir and Pikus strain Hamiltonian involve the following contributions (the zero terms are not listed below)

$$T_\varepsilon = \frac{P_0}{\sqrt{6}}\left(\varepsilon_{xx}k_1 + i\varepsilon_{yy}k_2\right),\ U_\varepsilon = \frac{P_0}{\sqrt{3}}\varepsilon_{zz}k_3, \tag{14}$$

$$\begin{aligned} Q_\varepsilon^{(001)} &= -b\left(\varepsilon_{xx} - \varepsilon_{zz}\right), \\ Q_\varepsilon^{(110)} &= \left(-\frac{b + \sqrt{3}d}{4}\right)\left(\varepsilon_{xx} - \varepsilon_{zz}\right), \\ Q_\varepsilon^{(111)} &= \frac{d}{\sqrt{3}}\left(\varepsilon_{xx} - \varepsilon_{zz}\right), \end{aligned} \tag{15}$$

$$R_\varepsilon^{(110)} = \left(\frac{\sqrt{3}b - d}{4}\right)\left(\varepsilon_{xx} - \varepsilon_{zz}\right) \tag{16}$$

The strain contributions, which are independent of orientation are the following: for valence band

$$P_\varepsilon = -a_v Tr\left(\varepsilon\right), \tag{17}$$

and for conduction band

$$E_\varepsilon^{CB} = a_c Tr\left(\varepsilon\right) \tag{18}$$

4.4. 8-band Hamiltonian

In this basis the rotated Hamiltonian is

$$\begin{pmatrix} A & 0 & \sqrt{3}T & -\sqrt{2}U & T^+ & 0 & U & -\sqrt{2}T^+ \\ 0 & A & 0 & -T & -\sqrt{2}U & -\sqrt{3}T^+ & -\sqrt{2}T & -U \\ \sqrt{3}T^+ & 0 & P+Q & -S & R & 0 & -\frac{S}{\sqrt{2}} & \sqrt{2}R \\ -\sqrt{2}U & -T^+ & -S^+ & P-Q & 0 & R & -\sqrt{2}Q & \sqrt{\frac{3}{2}}S \\ T & -\sqrt{2}U & R^+ & 0 & P-Q & S & \sqrt{\frac{3}{2}}S^+ & \sqrt{2}Q \\ 0 & -\sqrt{3}T & 0 & R^+ & S^+ & P+Q & -\sqrt{2}R^+ & -\frac{S^+}{\sqrt{2}} \\ U & -\sqrt{2}T^+ & -\frac{S^+}{\sqrt{2}} & -\sqrt{2}Q^+ & \sqrt{\frac{3}{2}}S & -\sqrt{2}R & P+\Delta & 0 \\ -\sqrt{2}T & -U & \sqrt{2}R^+ & \sqrt{\frac{3}{2}}S^+ & \sqrt{2}Q^+ & -\frac{S}{\sqrt{2}} & 0 & P+\Delta \end{pmatrix} \tag{19}$$

Standard definitions of terms of unrotated system are

$$
\begin{aligned}
P &= \frac{\hbar^2}{2m_0}\gamma_1(k_x^2+k_y^2+k_z^2) = \frac{\hbar^2}{2m_0}\gamma_1 k^2,\\
Q &= \frac{\hbar^2}{2m_0}\gamma_2(k_x^2+k_y^2-2k_z^2),\\
R &= \frac{\hbar^2}{2m_0}\left[-\sqrt{3}\gamma_2(k_x^2-k_y^2)+i2\sqrt{3}\gamma_3 k_x k_y\right],\\
S &= \frac{\hbar^2}{m_0}\gamma_3\sqrt{3}(k_x-ik_y)k_z
\end{aligned}
\tag{20}
$$

Matrix elements related to conduction band interactions are

$$\langle S|H|S\rangle = E_c + A'k^2 = A \tag{21}$$

Matrix elements for some particular orientations (001), (110), (111) are

$$A^{(001)} = A^{(110)} = A^{(111)} = A^{(112)} = A \tag{22}$$

The values of matrix elements Q, R and S depend on orientation. For selected orientations they are

$$Q^{(001)} = -\frac{\hbar^2}{2m_0}\gamma_2\left(k_1^2+k_2^2-2k_3^2\right) \tag{23}$$

$$
\begin{aligned}
Q^{(110)} &= -\frac{\hbar^2}{4m_0}\left(\gamma_2\left(2k_1^2-k_2^2-k_3^2\right)-3\gamma_3\left(k_2^2-k_3^2\right)\right),\\
Q^{(111)} &= -\frac{\hbar^2}{2m_0}\gamma_3\left(k_1^2+k_2^2-2k_3^2\right),\\
R^{(001)} &= \frac{\hbar^2}{2m_0}\sqrt{3}\left(\gamma_3\left(k_1^2-k_2^2\right)-i2\gamma_2 k_1 k_2\right),\\
R^{(110)} &= \frac{\hbar^2}{4m_0}\sqrt{3}\left(\gamma_2\left(2k_1^2-k_2^2-k_3^2\right)-\gamma_3\left[\left(k_2^2-k_3^2\right)+i4k_1k_2\right]\right),\\
R^{(111)} &= \frac{\hbar^2}{6m_0}\left(\sqrt{3}\left(\gamma_2+2\gamma_3\right)\left(k_1-ik_2\right)^2-2\sqrt{6}\left(\gamma_2-\gamma_3\right)\left(k_1+ik_2\right)k_3\right),\\
S^{(001)} &= \frac{\hbar^2}{m_0}\sqrt{\frac{3}{2}}\gamma_3\left(k_1-ik_2\right)k_3,\\
S^{(110)} &= \frac{\hbar^2}{m_0}\sqrt{\frac{3}{2}}\left(\gamma_3 k_1 k_3 - i\gamma_2 k_2 k_3\right),\\
S^{(111)} &= -\frac{\hbar^2}{6m_0}\left(\sqrt{3}\left(\gamma_2-\gamma_3\right)\left(k_1+ik_2\right)^2-\sqrt{6}\left(2\gamma_2+\gamma_3\right)\left(k_1-ik_2\right)k_3\right)
\end{aligned}
\tag{24}
$$

5. Numerical Approach

We start by expanding all position dependent terms in the Hamiltonian in the plane wave basis as

$$A(z) = \frac{1}{\sqrt{L}}\sum_m A_m e^{iK_m z},\ K_n = \frac{n\pi}{L}, \tag{25}$$

By multiplying from the left by

$$A(z) = \frac{1}{\sqrt{L}}\sum_m A_m e^{iK_m z},\ K_n = \frac{n\pi}{L}, \tag{26}$$

we arrive at an effective mass equation in plane wave basis of the form

$$[H]_{m',m}[f_{\alpha,m',(n)}] = E_{(n)}[f_{\alpha,m',(n)}] \tag{27}$$

Here, square brackets denote matrix and arrays in plane-wave basis. The n-th envelope eigenfunction is

$$F_n(z,k_p) = \frac{1}{\sqrt{L}}\sum_{\alpha,m} f_{\alpha,m,(n)}(k_p)e^{iK_m z} \tag{28}$$

6. Gain

In Fig. 7 we illustrate the origin of gain in an active system. External pump (in the case of semiconductor lasers the role is played by electric current) provides energy which is responsible for growth of photons.

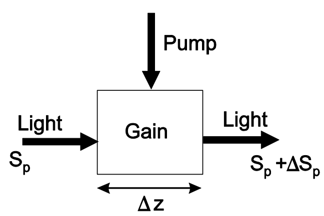

Fig. 7. Illustration of gain process.

Material gain was determined using a conventional method [20] based on the relaxation time approximation convoluted with a Lorentzian function with broadening time (0.1ps). In this approximation, the transverse electric (TE) gain is given by

$$g_\beta^{TE}(\omega) = C_0\beta^{-1}\sum_{n_c,n_v}\int dk\left[f_{n_c}(k)-f_{n_v}(k)\right] \times \sum_i |\langle\psi_{nc}|\varepsilon\cdot p_\alpha|\psi_{nv}\rangle|^2 L(n_c,n_v,k), \tag{29}$$

where $C_0 = q^2 / \left(m_0^2 \omega \tau c \varepsilon_0\right)$, q is elementary charge, m_0 is bare mass of an electron, ω is angular frequency, τ is a time constant, c speed of light, ε_0 dielectric constant and β propagation constant of the TE mode. Index i labels the heavy and light hole subbands, f_{nc} and f_{nv} are Fermi-Dirac distributions for n-th electron and hole subbands in the QW, respectively. They are given below

$$f_c\left(E_c(k), E_c^F\right) = \left(1 + \exp\left(\frac{E_c(k) - E_c^F}{k_B T}\right)\right)^{-1}, \quad f_v\left(E_v(k), E_v^F\right) = \left(1 + \exp\left(\frac{E_v(k) - E_v^F}{k_B T}\right)\right)^{-1} \tag{30}$$

where k_B is the Boltzmann's constant and T is the absolute temperature.

Various transitions between conduction band and valence bands which contribute to gain, Eq. (29) are illustrated in Fig. 8.

The squared optical transition matrix elements of TE mode which measure the transition between the hole subbands and the electron subbands are

$$|\langle\psi_{nc}|\varepsilon \cdot p_\alpha|\psi_{nv}\rangle|^2 = (M_{ci}^{TE})^2 \left|I_{n_v,i}^{n_c}(k)\right|^2, \quad \alpha = x, y, z \tag{31}$$

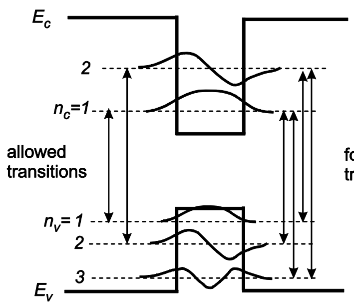

Fig. 8. Various transitions inside quantum well which contribute to material gain.

The overlap integral is defined as

$$\left|I_{n_v,i}^{n_c}(k)\right| = \int \psi_{nc}(k)\psi_{nv}(k)dz \tag{32}$$

The element M_{ci}^{TE} is evaluated for TE modes within dipole approximation. The broadening function is

$$L(n_c, n_v, k) = \frac{1}{\pi} \frac{\hbar / \tau}{\left(E_{eh} - E\right)^2 + \left(\hbar / \tau\right)^2} \tag{33}$$

Carrier densities in conduction (*N)* and valence (*P)* band are obtained as

$$N = \sum_{n_c} \int_0^{k_{max}} \rho(k) f_c\left(E_{n_c}(k), E_{CB}^F\right) dk, \tag{34}$$

$$P = \sum_{n_v} \int_0^{k_{max}} \rho(k)\left[1 - f_v\left(E_{n_v}(k), E_{VB}^F\right)\right] dk \tag{35}$$

Material gain was evaluated for several carrier densities. For each density we have determined the quasi-Fermi levels E_{CB}^F and E_{VB}^F for the CB and VB, respectively. The carrier density in a given band of the QW is defined by integration of the product of density of states, *ρ (k,z):*

$$\varrho(k,z) = \frac{kT}{\pi\hbar^2} \sum_{m_{s,\alpha}} \left|I_{n_v,i}^{n_c}(k)\right|^2 \frac{1}{1+\exp(\frac{E_{c,f}^F}{kT})}, \tag{36}$$

and occupation probability of carriers (i.e., the Fermi-Dirac distribution) over the entire band. For non-parabolic bands, the integration is carried out in ***k*** space with the density of states determined from ***kp*** calculations. k_{max} is the integration limit determined by the convergence of integrals used to determine *N* and *P*.

7. Results

Calculations were performed for 7 nm quantum wells made of $In_{0.36}Ga_{0.64}As_{0.973}$ $N_{0.027}$ /GaAs. Our numerical approach was described in an earlier Section. All parameters which depend on compositions were obtained using linear interpolation.

Some of the results are summarized in Figs. 9 and 10. All results are compared with a standard direction (001). In Fig. 9 we show band dispersion, i.e., dependence of energy vs k-vector.

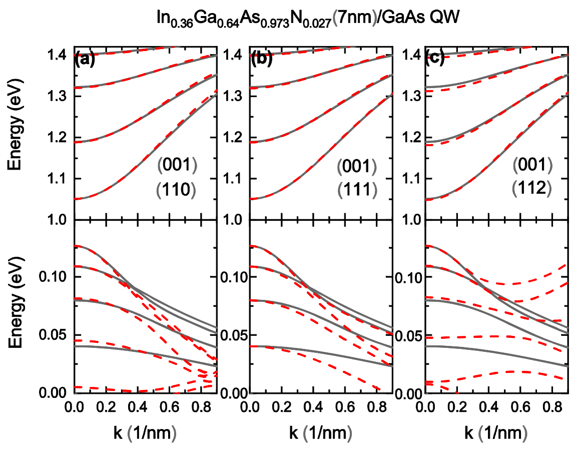

Fig. 9. Band structure calculated for $In_{0.36}Ga_{0.64}As_{0.973}$ $N_{0.027}$ /GaAs QW grown on directions: (a) (001) gray line, (110) red line, (b) (001) gray line, (111) red line, (c) (001) gray line, (112) red line.

One can observe that results of the band structure calculations show significant differences for substrates oriented along (110), (111) and (112) with respect to (001) direction. Differences in the band structure are particularly significant for the valence band. One can notice that for each direction effective masses of holes differ from the (001) direction. The changes in the conduction band for different directions are relatively small.

Some of the results of the material gain spectra are shown in Fig. 10. The calculations were performed for carrier concentrations ranging from 1×10^{18} cm^{-3} to 6×10^{18} cm^{-3}. The maximum gain values, dependent on carrier concentration, are illustrated in Fig. 11.

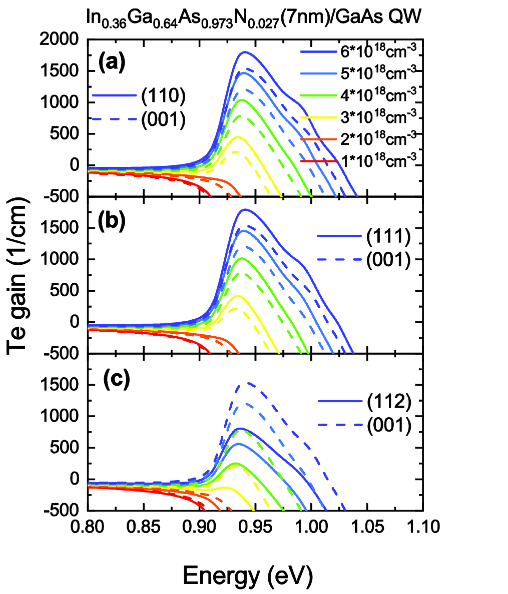

Fig. 10. Material gain calculated for $In_{0.36}Ga_{0.64}As_{0.973}$ $N_{0.027}$ /GaAs QW grown on directions: (a) (001) dash line, (110) solid line, (b) (001) dash line, (111) solid line, (c) (001) dash line, (112) solid line. Calculations were performed for carrier concentrations from $1\text{x}10^{18}$ cm^{-3} to $6\text{x}10^{18}$ cm^{-3}.

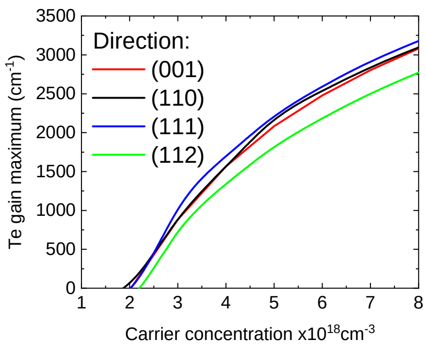

Fig. 11. Gain peak for TE mode vs carrier's concentration for various directions of growth.

Notably, there are discernible differences in the gain values calculated for various crystallographic orientations. Specifically, directions (110) and (111) yield higher values compared to the standard (001) direction, while direction (112) results in smaller values. This correlation is attributed to the band structure calculations. The curves in the valence bands exhibit an upward trend, which is associated with lower gain values. The changes in carrier distribution within the valence band are depicted in Fig. 12. Carrier distributions were precisely computed using the Eqs. (34) and (35), with density of states determined from Eq. (36), with a fixed carrier concentration of 5×10^{18} cm^{-3} for each direction, namely, (001), (110), (111), and (112). The color map, transitioning from blue to red, represents carrier localization calculated under each scenario. Fig. 12 also includes the potential shape in the valence band and the hole Fermi level calculated for the given carrier concentration.

8. Conclusions

In this paper we described method of determining band structure and material gain for $In_{0.36}Ga_{0.64}As_{0.973}$ $N_{0.027}$ /GaAs material system on arbitrary oriented substrates. We used the 8-band kp method. We presented general expressions for arbitrary orientations of the substrate. Detailed results of band structure are shown for quantum wells grown on (001)-, (110)-, (111)- and (112)-oriented substrates. Band structure depends on the direction of growth as well as resulting strain changes.

Our results indicate that for $In_{0.36}Ga_{0.64}As_{0.973}$ $N_{0.027}$/GaAs quantum wells and carrier concentrations $1-6\times10^{18}cm^{-3}$ (typical for semiconductor lasers) gain spectra are affected by orientation of the substrate. One observes an increase of gain peak (compared to (001) orientation) for (110) and (111) directions.

As shown by our simulation results, the growth direction significantly affects band structure and also material gain. Therefore, it can be considered as an additional parameter used in the design and optimization of optoelectronic devices.

References

[1]. J. Ohtsubo, Semiconductor Lasers. Stability, Instability and Chaos, *Springer*, 2017.

[2]. T. Numai, Fundamentals of Semiconductor Lasers, *Springer*, 2015.

[3]. G. P. Agrawal, N. K. Dutta, Semiconductor Lasers, 2nd Ed., *Van Nostrand Reinhold*, 1993.

[4]. R. Kudrawiec, D. Hommel, Bandgap engineering in III-nitrides with boron and group V elements: Toward applications in ultraviolet emitters, *Applied Physics Review*, Vol. 7, 2020, 041314.

[5]. I. S. Tarasov, High-power semiconductor separate-confinement double heterostructure lasers, *Quantum Electronics*, Vol. 40, 2010, 661.

[6]. P. P Vasil'ev, I. H White, J. Gowar, Fast phenomena in semiconductor lasers, *Reports on Progress in Physics*, Vol. 63, 1997, 63.

[7]. M. Kucharczyk, M. S. Wartak, P. Weetman, P.-K. Lau, Theoretical modeling of multiple quantum well lasers with tunneling injection and tunneling transport between quantum wells, *Journal of Applied Physics*, Vol. 86, 1999, 3218.

[8]. J. Dong, L. Zhang, X. Dai, F. Ding, The epitaxy of 2D materials growth, *Nature Communications*, Vol. 11, 2020, 5862.

[9]. A. T. Meney, Orientation dependence of subband structure and optical properties in GaAs-AlGaAs quantum wells:[001], [111], [110] and [310] growth directions, *Superlattices and Microstructures*, Vol. 11, 1992, pp. 31-40.

[10]. A. T. Meney, Effects of growth direction on lasing performance in $GaAs-Al_x Ga_{1-x} As$ quantum wells, *Superlattices and Microstructures*, Vol. 11, 1992, pp. 387-392.

[11]. A. Niwa, T. Ohtoshi, T. Kuroda, Orientation dependence of optical properties in long wavelength strained quantum-well lasers, *IEEE Journal of the Selected Topics in Quantum Electronics*, Vol. 1, 1995, pp. 211-217.

[12]. T. Ohtoshi, T. Kuroda, A. Niwa, S. Tsuji. Dependence of linewidth enhancement factor on crystal orientation in strained quantum well lasers, *Photonics Technology Letters*, Vol. 6, 1994, pp. 1424-1426.

[13]. W. Shan, W. Walukiewicz, J. W. Ager III, E. E. Haller, J. F. Geisz, D. J. Friedman, J. M. Olson, S. R. Kurtz, Band Anticrossing in GaInNAs Alloys, *Physical Review Letters*, Vol. 82, 1999, 1221.

[14]. W. Shan, W. Walukiewicz, K. Yu, J. Ager, E. Haller, J. Geisz, D. Friedman, J. Olson, S. Kurtz, H. Xin, C. Tu, Band anticrossing in III-N-V alloys, *Physica Status Solidi B-basic Research*, Vol. 223, 2001, pp. 75-85.

[15]. S. T. Ng, W. J. Fan, Y. X. Dang, S. F. Yoon, Comparison of electronic band structure and optical transparency conditions of $In_x Ga_{1-x} As_{1-y} N_y$/Ga As quantum wells calculated by 10-band, 8-band, and 6-band k· p models, *Physical Review B*, Vol. 72, 2005, 115341.

[16]. M. Gladysiewicz, R. Kudrawiec, J. M. Miloszewski, P. Weetman, J. Misiewicz, M. S. Wartak, Band structure and the optical gain of GaInNAs/GaAs quantum wells modeled within 10-band and 8-band kp model, *Journal of Applied Physics*, Vol. 113, 2013, 063514.

[17]. M. Gladysiewicz, M. S. Wartak, On the Effect of Substrate Orientation on the Properties of Quantum well Semiconductors, in *Proceedings of the 5th International Conference on Microelectronic Devices and Technologies (MicDAT'2023)*, Funchal (Madeira Island), Portugal, 20-22 September 2023, pp. 42-46.

[18]. M. Gladysiewicz, M. S. Wartak, Effect of substrate orientation on band structure of bulk III-V semiconductors, *AIP Advances*, Vol. 12, 2022, 115208.

[19]. G. L. Bir, G. E. Pikus, Symmetry and Strain-Induced Effects in Semiconductors. *Wiley*, 1974.

[20]. S.-L. Chuang, Physics of Optoelectronic Devices *Wiley*, 1995.

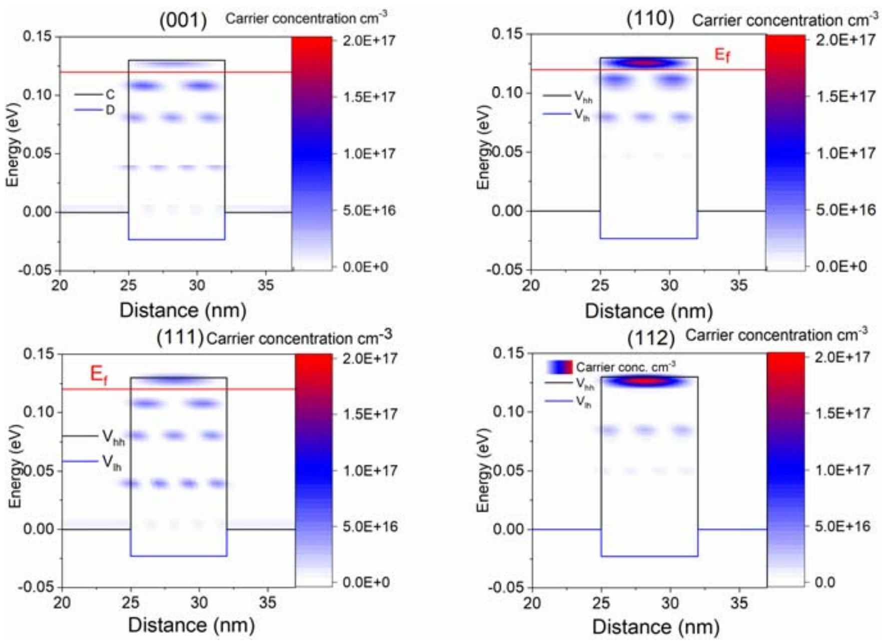

Fig. 12. Carrier distribution (P) as a function of distance and energy for substrates oriented along (001), (110), (111), and (112). These calculations were performed for a fixed carrier concentration of 5×10^18 cm⁻ ³. The red line represents the Fermi level's position within the valence band.